



Contents lists available at ScienceDirect

International Journal of Psychophysiology

journal homepage: www.elsevier.com/locate/ijpsycho

Combining fMRI with EEG and MEG in order to relate patterns of brain activity to cognition

Walter J. Freeman^{a,*}, Seppo P. Ahlfors^{b,1}, Vinod Menon^{c,2}

^a Department of Molecular & Cell Biology, University of California MC 3206, Berkeley CA 94720 USA

^b MGH/MIT/HMS Athinoula A Martinos, Center for Biomedical Imaging, Massachusetts General Hospital, 149 13th St., Mailcode 149-2301, Charlestown MA 02129, USA

^c Department of Psychiatry & Behavioral Sciences and Program in Neuroscience, Neuroscience Institute at Stanford, Stanford University School of Medicine, Stanford, CA 94305-5778, USA

ARTICLE INFO

Article history:

Received 16 August 2008

Received in revised form 26 November 2008

Accepted 23 December 2008

Available online xxxx

Keywords:

Analytic amplitude

Black noise

Criticality

ECoG

EEG

fMRI

Ground state

MEG

Mesoscopic cortical activity

Power spectral density

PSD

Resting state

Spatial AM pattern

ABSTRACT

The common factor that underlies several types of functional brain imaging is the electric current of masses of dendrites. The prodigious demands for the energy that is required to drive the dendritic currents are met by hemodynamic and metabolic responses that are visualized with fMRI and PET techniques. The high current densities in parallel dendritic shafts and the broad distributions of the loop currents outside the dendrites generate both the scalp EEG and the magnetic fields seen in the MEG. The measurements of image intensities and potential fields provide state variables for modeling. The relationships between the intensities of current density and the electric, magnetic, and hemodynamic state variables are complex and far from proportionate. The state variables are complementary, because the information they convey comes from differing albeit overlapping neural populations, so that efforts to cross-validate localization of neural activity relating to specified cognitive behaviors have not always been successful. We propose an alternative way to use the three methods in combination through studies of hemisphere-wide, high-resolution spatiotemporal patterns of neural activity recorded non-invasively and analyzed with multivariate statistics. Success in this proposed endeavor requires specification of what patterns to look for. At the present level of understanding, an appropriate pattern is any significant departure from random noise in the spectral, temporal and spatial domains that can be scaled into the coarse-graining of time by fMRI/BOLD and the coarse-graining of space by EEG and MEG. Here the requisite patterns are predicted to be large-scale spatial amplitude modulation (AM) of synchronized neuronal signals in the beta and gamma ranges that are coordinated but not correlated with fMRI intensities.

© 2009 Elsevier B.V. All rights reserved.

1. Introduction

1.1. fMRI, neural activity and brain energetics: statement of the problem

Brains as thermodynamic systems consume energy at rates roughly ten-fold greater than any other organ of comparable mass. The high rates hold whether subjects are at rest or active, leading to the sobriquet “dark energy” (Raichle, 2006) in analogy to the preponderance of inscrutable astronomical mass-energy. This difference in rates of energy dissipation is closely related to that between the metabolic rates of homeotherms vs. poikilotherms. Maintenance of high constant body temperature gives an unequivocal advantage to birds and mammals in the struggle for survival, despite the ten-fold increase in the cost of dissipated metabolic energy. Similarly, the high

metabolic rate in brains is necessary to maintain the ionic energy reserves at self-organized criticality (Freeman, 2008), a critical state of readiness to cope with environmental vicissitudes, whatever the metabolic cost.

That readiness is based in the background activity, which has been shown to arise by mutual excitation among cortical excitatory neurons (reviewed in Freeman, 2008). The intensity of the background activity varies with the degree of arousal, but the stability at every level and in every location is maintained by the refractory periods, not by inhibition or thresholds (Freeman, 2007b). The role of inhibition is to impose spatiotemporal order and structure on the otherwise random noise background activity. The transition from behavioral rest to intentional action invokes reorganization of the background activity that may increase, decrease or not change the mean level of activity. What is expected to change is the emergence of spatiotemporal patterning by local increases and decreases of energy dissipation from the background levels. Obviously in the continuous interactions of excitatory and inhibitory neurons the coincidence of excitatory and inhibitory currents in the same dendritic trees must at least partially cancel the extracellular electric and magnetic fields, but the metabolic

* Corresponding author. Tel.: +1 510 642 4220.

E-mail addresses: dfreeman@berkeley.edu (W.J. Freeman), seppo@nmr.mgh.harvard.edu (S.P. Ahlfors), menon@stanford.edu (V. Menon).

¹ Tel.: +1 617 726 0663.

² Tel.: +1 650 498 6737.

demands must still be met for both forms of activation and for all frequency ranges. The resulting dissipation of energy resources, as well as the disparity in manifestations, is likely to be highest in the high frequency ranges, where phase dispersion with fixed axonal delays is maximal, and where the density of neural information is likely to be highest, but where resolution with fMRI is not possible.

This cancellation focuses the problem to be solved for fMRI, which is to relate local cerebral blood flow to local neural activity. The basic relation in the simplistic view is that the capillaries open in brain areas in which CO₂ has accumulated as the by-product of neurons burning glucose. The relation in one respect is simpler than in other organs, because brain arterioles lack the muscular cuff by which neural control can over-ride local control by CO₂, especially in pre-adaptation of blood flow to predicted onset of muscular exercise vs. digestion. However, the CO₂ combines locally with water by the enzyme carbonic anhydrase as carbonic acid, which then dissociates. It is unclear whether the capillaries respond directly to the CO₂ or to the acid (pCO₂ versus pH) or both. Moreover, the astrocytes in cortex hold a substantial reservoir of glycogen (“animal starch”), which is a ready local source of glucose that can be split without oxygen, giving pyruvic and lactic acids without producing CO₂ (anaerobic metabolism), in which instances neural activity might be dissociated from blood flow and blood oxygen level dependent (BOLD) signals for extended time periods until the oxygen debt is repaid.

The homeostatic feedback that regulates the local pCO₂ or pH is likely to be based regionally on the vascular architectures and its coupling to glial circuits (Schummers et al., 2008) rather than the neural architectures, which varies among cortical regions. Astrocytes, the most abundant glial cells, are not only metabolically coupled to neighboring neurons but also communicate directly with the vasculature. Astrocytic activity affects local blood flow, which can be assessed by noninvasive hemodynamic mapping techniques such as intrinsic signal optical imaging (Arieli and Grinvald, 2002). The relation between neuronal networks, astrocytes, and hemodynamic responses is an important topic of on-going research (Wolf and Kirchhoff, 2008). Resolution of this problem would appear to require detailed comparisons of the vascular and neural architectures of local cortical regions that have been located by simultaneous measurements of glycogen depletion, pO₂, pCO₂ and pH in conjunction with blood flow and, most revealingly, neural activity that has been classified by spatiotemporal neural activity patterns with respect to specific cognitive behaviors.

Further complications ensue from the fact that the activity of inhibitory neurons also requires metabolic energy, and so also does the maintenance of inhibitory synaptic potentials by excitatory neurons (Buzsáki et al., 2007; Logothetis, 2008). Since 95% of cortical energy is expended by dendrites and 5% by axons, the reduction in transmission of action potentials by excitatory neurons cannot compensate for the augmented dissipation necessitated by inhibition. The level of “activity” revealed by hemodynamic imaging alone must inescapably include both excitation and inhibition. However, in the identification of macroscopic spatiotemporal patterns, the localization of peaks and troughs to cortical landmarks is secondary to the classification of the field patterns with respect to intentional behavior, as prelude to correlation with respect to anatomical landmarks. The problem for interpretation of hemodynamic images can then be seen to require coordination not correlation with electric and magnetic measurements of excitation and inhibition in neuron populations across disparate scales of space and time.

1.2. Complementarity of EEG, MEG, and fMRI signals

Multivariate approaches for characterizing and decoding local and distributed neuronal activity patterns in fMRI have been receiving increased attention in recent years. Multivoxel pattern analyses of fMRI and BOLD signals are being used to circumvent conceptual and

methodological limitations of the localization approach to brain imaging (Logothetis, 2008). Spatial patterns of brain activity can have significantly greater sensitivity and specificity for detecting conscious and unconscious mental processes than activity in individual regions (Haynes and Rees, 2006; Soon et al., 2008). This newfound emphasis in fMRI research on classification and pattern recognition, which is the focus of our proposed approach, will undoubtedly facilitate a more integrated approach to linking perceptually relevant representations of fMRI, EEG and MEG neuronal signals by highlighting their functional complementarity. The most important insight is that the neural correlates of cognitive load are likely to be found in the large-scale, widely distributed, spatially coherent neural activities at the mesoscopic and macroscopic levels, as defined below. At the systems level the problems encountered in attempts at spatial localization and the precise descriptions of microscopic causal relations are secondary. Our first task is to measure and model these transiently coherent spatiotemporal patterns.

For direct correlation of fMRI with EEG and MEG the limitations of resolution of fMRI must be considered. Only the fMRI images of cortical activity are admissible for the correlation, owing to the limits on the class of neurons that can contribute to signals derived from the EEG and MEG, as discussed below. On the one hand the spatial resolution of fMRI reaches into the mm range, which is appropriate for cortical thickness in humans ranging from 1 to 4 mm. Matching the image of enhanced blood flow to the thickness of the cortical neuropil poses a strict criterion for localization that is not often met by any of the several methods. On the other hand, the temporal resolution of fMRI inherently limits correlations to spatial patterns of EEG and MEG that have been averaged over the several seconds that characterize the time resolution of changes in the metabolic and vascular responses of cortex to metabolic demands for the removal of waste CO₂, acid, and heat. The need for time averaging unavoidably invokes the necessity to deal explicitly with a hierarchy of neural activity in cognition, not only with the microscopic action potentials but also with the macroscopic field potentials of the EEG and MEG.

An optimal way to construct feature vectors for classification of spatial AM patterns would be to combine estimates of analytic power in frames from both EEG and MEG. Feature vectors defined below might then be constructed from all available sources to represent patterns of mean excitation, inhibition, and energy dissipation over the time spans are needed to estimate fMRI images reliably. To accomplish this the data must be spatially coarse-grained to conform to the spatial resolution specified by the spatial intervals of the sensors in the arrays used for EEG and MEG recordings and temporally coarse-grained to conform to the temporal frequencies provided by sequential hemodynamic imaging. The most valuable tool is the spatial power spectral density (PSD_x), which has been calculated for the scalp EEG (Freeman et al., 2003b), intracranial human electrocorticogram (ECoG, Freeman et al., 2000) and fMRI (Worsely, 2005) but surprisingly not for MEG.

Temporal summation alone cannot suffice, because spatial images of dissipation given by analytic power from the EEG and MEG are specific for the temporal spectral pass bands, whereas fMRI is indiscriminate in that respect. The obvious remedies are to combine the spatial patterns over the several available temporal pass bands, and to conduct analysis of variance to determine which pass bands of analytic power might correspond to selected components of fMRI from two or more sequential behavioral states. This approach avoids subtracting control and test images in search of localization. As discussed below, in many physical systems the rate of energy dissipation is inversely proportional to the square of the frequency of oscillation. This relation is most clearly seen by graphing the temporal power spectral density (PSD_T) in coordinates of log₁₀ power vs., log₁₀ frequency. Such systems are said to generate “brown noise” with 1/f² power-law PSD (slope of -2). For example, the theta power spectral density at 4 Hz is 100 times the gamma power spectral

194 density at 40 Hz, while the power dissipations at 4 Hz and 40 Hz are
 195 equal. The utility of EEG and MEG data might be greatest in helping to
 196 decompose fMRI into identifiable frequency ranges of dissipation
 197 related to cognitive behaviors. For example, the fMRI might locate
 198 cortical areas in which the amplitudes of EEG and MEG oscillations are
 199 quite low. If the metabolic demand is low, then the neural activity is
 200 low. If the blood flow is high, the relative silence implies active
 201 silencing by inhibition. If it is very high, it may signify the furious
 202 dissipation of neural energy by the cancellation of strong excitatory
 203 and inhibitory synaptic currents in a situation that is metabolically
 204 very expensive indeed and perhaps restricted to a narrow pass band,
 205 or perhaps not. Then the problem to be solved for fMRI interpretation
 206 emerges in predicting the forms of spatiotemporal patterning
 207 revealed by EEG and EMG, such that they can be measured and
 208 averaged over time and space without loss of the essential features in
 209 the process of averaging. That is the problem addressed in the
 210 remainder of this essay.

211 2. The several manifestations of cortical dendritic current in fMRI, 212 EEG and MEG

213 2.1. Foundation of non-invasive brain imaging in neural energy

214 Human brain activity can be monitored non-invasively at and
 215 above the scalp based on the production by intracranial neurons of
 216 electric and magnetic fields. The fields accompany the electric current
 217 by which dendrites sum and communicate their synaptic input to the
 218 trigger zones of the single, often many-branched axon by which each
 219 neuron transmits its output to other neurons more or less distant. The
 220 frequencies of oscillation in the intensities of the fields are much too
 221 low to generate significant electromagnetic radiation (radio waves),
 222 and the wavelengths are kilometers long, so the intensities of fields
 223 are measured separately as the EEG and MEG.

224 The energy that drives the electric current is immediately provided
 225 by chemical gradients of ions, particularly those for sodium and
 226 potassium, which ionic pumps sustain across neural membranes. That
 227 chemical energy is held in a vast reservoir that is instantly available at
 228 all times like a battery to drive current at the flip of a synaptic switch.
 229 After each use that store of energy is replenished by relatively slow
 230 metabolic processes, which require the cerebrovascular system to
 231 deliver oxygen and glucose and remove carbon dioxide and heat. The
 232 modifications in local rates of cerebral blood flow that accompany
 233 changes in neural activity are detected and imaged by hemodynamic
 234 and metabolic techniques (Logothetis, 2008). The three signals, EEG,
 235 MEG, and fMRI, can either increase or decrease in relation to
 236 behavioral and cognitive demands, thereby forming spatial patterns
 237 in brain images. Because inhibition is an active process that requires
 238 expenditure of metabolic energy, “activation” and “deactivation”
 239 differ radically from “excitation” and “inhibition”.

240 2.2. Differing sensitivities of electromagnetic and hemodynamic measures

241 All three types of non-invasive brain imaging methods reveal
 242 different aspects of global neural activity. The EEG and MEG manifest
 243 the activity of only a limited class of neurons. First, the neurons must
 244 have a degree of axial symmetry, meaning that the activated dendrites
 245 must lie to one side of the cell body and axon, so that the sites of current
 246 outflow (*sources*) are spatially separated from the sites of current inflow
 247 (*sinks*). Typically these are pyramidal cells, which generate dipole fields
 248 that can extend throughout the brain and beyond. Cortical interneurons
 249 typically have radial symmetry (*stellate cells*), so their sources and sinks
 250 intermingle, and their distant fields cancel. The local field potentials
 251 (LFP) within their dendritic branches are designated as *closed*; they
 252 cannot contribute significantly to the EEG or MEG at or above the scalp,
 253 or even to electric fields recorded with electrodes on exposed pial
 254 surfaces, the electrocorticogram (ECoG). The syncytia formed by gap

255 junctions also typically generate closed fields. The fields are dendritic in
 256 origin; axons clearly mediate the strengths of dendritic currents by the
 257 information they transmit, but their action potentials do not contribute
 258 directly to the dendritic potentials, certainly not as “envelopes of spikes”
 259 except when artificially synchronized by impulse stimuli. Second, the
 260 neurons must be aligned in palisades, both the dendrites in cortical
 261 columns perpendicular to the pial surface and the cell bodies in layers
 262 parallel to the pial surface. The cellular architectures of nuclei and
 263 reticular networks that lack the laminar organization of cortex seldom
 264 support the spatial summation of multineuronal dipole fields that is
 265 required for significant oscillations to appear at the scalp. Third, the
 266 contributing neurons must support strong local interactions probably by
 267 gap junctions in some areas and certainly by local and distant
 268 interactions through axodendritic synapses in all areas, in order to
 269 provide the temporal synchrony necessary for sufficiently broad
 270 summation for the potential fields to appear at the scalp.

271 Thus, while fMRI and BOLD can image neural activities in all cortical,
 272 nuclear and reticular architectures predominantly containing dendrites,
 273 EEG and MEG are largely restricted to imaging activities of cerebral
 274 cortex but not cerebellar cortex. Purkinje cells also have a columnar and
 275 laminar structure that could, theoretically, permit neuronal sources in
 276 the cerebellum to also contribute to scalp EEG. However, the cerebellum
 277 does not contribute significantly to EEG signals, because of the extreme
 278 curvature of its gyri tending to form closed fields, the sparseness of the
 279 Purkinje cells, and the predominance of feedforward inhibition over
 280 feedback inhibition. Forward inhibition promotes spatial differentiation,
 281 not the integration that gives broad fields of synchronized oscillations
 282 provided by feedback inhibition and forward excitation. Likewise,
 283 neuronal sources in structures such as the thalamus and basal ganglia
 284 have a radial, non-columnar organization, so are less likely to make any
 285 significant contributions to the scalp EEG even when intense LFP can be
 286 recorded within them (Niedermeyer and Lopes da Silva, 2004). The fMRI
 287 signals do not depend on the laminar or the radial neuronal
 288 organization, but have more to do with the coupling of metabolic
 289 processes to the underlying vascular and glial beds (Fox et al., 1988;
 290 Menon and Crottaz-Herbette, 2005; Herrmann and Debener, 2008).

291 All three methods give access to wide areas of cortex in a virtual
 292 continuum over the calvarium, albeit with differing degrees of spatial
 293 and temporal resolution. All three give 2-D images of spatial patterns of
 294 neural activity that change with time, some of which are expected to
 295 correlate with specific cognitive behaviors. Therefore, the cortical fMRI
 296 and EEG and MEG offer opportunities for mutual validation of behavioral
 297 correlates. In a simplistic view the rate of energy dissipation that is
 298 required to generate dendritic current should rise in proportion to
 299 current density and therefore the amplitudes of EEG and MEG potential
 300 differences; so likewise on a longer time scale should the rate of tissue
 301 perfusion needed to replenish the ionic energy reservoir. Studies reflect
 302 that expectation by combining imaging and physiology experiments in
 303 monkeys, indicating that the fMRI signals are more closely correlated
 304 with EEG, ECoG and LFP than with multiunit and single neuron activity
 305 (Logothetis and Pfeuffer, 2004), and that neurometabolic coupling in
 306 cerebral cortex reflects dendritic activity more than axonal activity
 307 (Viswanathan and Freeman, 2007). LFP in the high gamma band
 308 (>40 Hz) are better and more reliable predictors of the BOLD signal
 309 (Goense and Logothetis, 2008). However, the mechanisms of the
 310 relations between electrical oscillations and the concurrent fMRI signals
 311 are not yet known in sufficient detail to integrate reliably. Predictions are
 312 needed of what forms the cognitively related activities take, such that
 313 the signals can be combined across the differences in time and space
 314 scales. This is not a trivial problem. Solution requires a deep under-
 315 standing of the hierarchical organization of brain activity.

216 2.3. Differences between analyses of neural modules and neural fields

317 A useful hierarchy of brain signals and levels of organization is
 318 based on techniques of observation. The predominant signals that are

319 detected by microelectrodes inserted into cortex are the trains of
 320 action potentials from neurons that can be studied individually as
 321 components of networks and modules. The signals and the neurons
 322 are microscopic. The predominant signals that are recorded from
 323 arrays of depth electrodes, the LFP, and from arrays of electrodes on
 324 the cortical surface, the ECoG, are sums of potentials generated by
 325 cooperative interactions among very large assemblies. The signal from
 326 each electrode comes from at least 10,000 neurons and typically many
 327 more. These self-organized neural masses are continuous in space,
 328 and likewise the signals they generate are spatially continuous. The
 329 neural masses are fields that embed the networks and modules
 330 forming the primary sensory and motor cortices and components of
 331 the limbic system. They constitute the mesoscopic level of brain
 332 function. The effects of the fields on the neural networks and modules
 333 that they embed are only apparent in statistical averages of the
 334 microscopic activity. Lastly, the signals that emerge from the head in
 335 the EEG and MEG originate in neural masses that vary structurally and
 336 functionally in size and complexity, up to the entire cerebral
 337 hemisphere. These signals are from neural fields that are very large
 338 indeed, characteristically being difficult to distinguish from referential
 339 activity and volume conduction, yet providing insight into the global
 340 organization of brain activity. This is the macroscopic level given by
 341 EEG and MEG and fMRI from the continuous sheet of neuropil in each
 342 cerebral hemisphere in which the microscopic networks and modules
 343 are embedded along with the intermediate mesoscopic assemblies. It
 344 is apparent that networks and modules are functional entities with
 345 variable size and adaptive boundaries being re-defined by the
 346 mesoscopic and macroscopic fields of brain activity with each new
 347 cognitive task and within tasks from each tenth of a second to the
 348 next.

349 The neocortex provides many specialized areas that provide
 350 substrates for locally self-organized modules. The most widely held
 351 hypothesis of cortical function is that each module generates its
 352 characteristic signal; that these signals intermingle by volume
 353 conduction; that separation might be achieved by decomposition
 354 with independent component analysis (ICA); and that intermittent
 355 transmission among modules is manifested by transient phase-
 356 locking of microscopic or mesoscopic oscillations with zero phase
 357 lags despite axonal propagation delays on temporary connections
 358 (e.g., Singer, 2001; Makeig et al., 2002; Bressler et al., 2007). Our
 359 thermodynamic hypothesis, which is loosely related to Baars' (1997)
 360 "global workspace", is that self-organized modules are embedded in
 361 the cortical neuropil; that they enter by phase transitions into
 362 transient frames of synchronized oscillations having narrow spectral
 363 bands and broad spatial distributions; that the oscillation in the pass
 364 band of each frame is modulated in amplitude (AM) and phase (PM);
 365 that multiple frames coexist in narrow pass bands in the beta and
 366 gamma ranges; and that frames can be separated by spectral decom-
 367 position. The role of fMRI in this schema is to provide the macroscopic
 368 frame for the cortical events occurring in a 4 to 5 s window during a

reproducible cognitive task. There is increasing evidence that areas of
 high and low blood flow form spatial patterns of PET and fMRI (Raichle
 et al., 2001; Greicius et al., 2003; Fransson, 2006; Morcom and
 Fletcher, 2007; Raichle and Snyder, 2007; Schacter and Addis, 2007;
 Szpunar et al., 2007). The roles of EEG and MEG are to provide non-
 invasive measurements at high spatial and temporal resolution
 throughout the corresponding spatial and temporal window, and
 with repetition as often as needed to achieve statistical synthesis and
 verification in respect to fMRI.

3. Search for control states in fMRI, EEG and MEG

3.1. Definitions of "resting" and "ground" states

Many fMRI studies are based on comparison of spatial patterns
 between an active behavior and the control state without that
 behavior. Yet brains are always active. The study of the background
 activity forces this vexing problem (Raichle et al., 2001; Freeman,
 2004a,b, 2005a,b, 2006). What is the baseline from which changes in
 activity levels are to be measured? How might a non-cognitive
 "resting" state or a "ground" state for brain activity best be defined?
 Must "activation" carry populations above the level of either state, or
 might "activation" include reductions below either state? If so, how,
 and with what advantage?

Our path to understanding spatiotemporal patterns in scalp EEG
 and MEG began with analysis of the spatiotemporal properties of the
 ECoG in human (Freeman et al., 2006; Panagiotides et al., 2008) and
 animal (Freeman, 2004a,b). For the extraction of the relevant AM
 patterns, the ECoG must be recorded with multielectrode arrays fixed
 on the flattened pial surface of cortex that provide the necessary
 window for observation and measurement. Examination of the
 background *spontaneous* ECoG in animals and humans has shown
 that the only unambiguously defined basal level for energy and neural
 activity is the absence of oscillation and action potentials giving *flat*
EEG. This state is fully reversible when it is induced in some animals by
 hibernation and in others by very deep surgical anesthesia, ther-
 apeutically suppressing neural interactions. It corresponds to the *open*
loop state (Freeman, 1975), in which the mesoscopic time and space
 constants of the dendrites of neural populations can be measured.
 From this *vacuum* state (Freeman and Vitiello, 2006) there is a graded
 return through slow wave coma and chaotic waking rest to expectant
 arousal, with culmination in engagement in intentional action (Skarda
 and Freeman, 1987; Freeman, 2008). The stages of arousal resemble
 those in waking from slow-wave sleep; they are discriminable with
 soft criteria.

Of particular interest is the *resting* state, in which subjects are
 behaviorally inactive and unchallenged by immediate expectation of a
 conditioned stimulus (CS) and its attendant conditioned response
 (CR), eyes closed or open. As observed in humans this state is
 accompanied with a remarkably reproducible pattern of increased

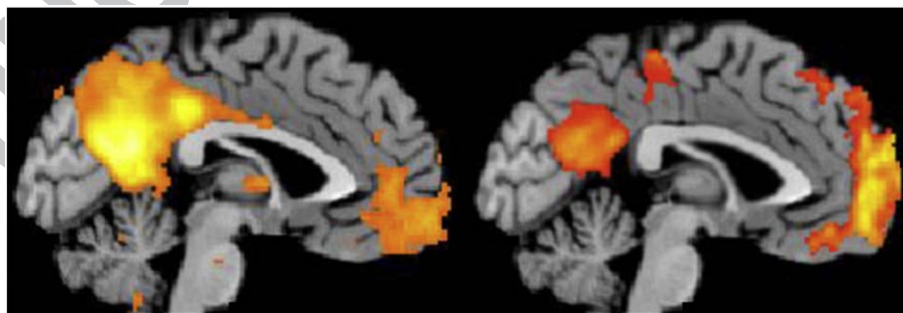


Fig. 1. (Left) Independent Components Analysis of "passive" resting-state fMRI scans shows spatially coherent activity in the posterior cingulate cortex, precuneus and medial prefrontal cortex nodes of the default mode network. (Right) Transient fMRI signal reductions are revealed during an auditory "oddball" attention task in these same regions. Unpublished data (Menon).

metabolic activity in midline brain structures, notably the ventromedial prefrontal cortex and the posterior cingulate cortex, documented in humans at rest (Shulman et al., 1997) with closed eyes and presumably empty minds. In view of its reproducibility during task based deactivations Raichle labeled it as a “default mode” (Raichle et al., 2001); reviewed by (Raichle and Snyder, 2007). These regions are found to be highly correlated with each other and therefore are hypothesized to constitute a default mode network (Greicius et al., 2003). Embarkation from the default state to overt action is accompanied by increases in neurometabolic demands in some brain regions and decreases in others. The neural mechanisms of the decreases and their functional significance are matters for conjecture and controversy (Morcom and Fletcher, 2007), and likewise the mental contents of subjects at rest in the default mode (Buckner et al., 2008). Raichle et al. and Greicius et al. defined their reference state with respect to behavioral and hemodynamic changes (Fig. 1). The uncertainty inherent in this definition is apparent in comparing the pattern with those demonstrated by others (Raichle and Snyder, 2007; Szpunar et al., 2007) accompanying the cognitive functions of recollection and prediction, showing substantial overlap, which suggests that “resting” may be indistinguishable from “occult cogitating” by these criteria. This holds likewise for imaging correlates of “self-referential processing” (Northoff et al., 2006).

A complementary approach is to seek in the EEG the characteristic power spectral density (PSD) of the ECoG, EEG or MEG that is recorded from subjects similarly showing no overt or imminent behaviors. The time series from multiple electrodes in this state often yield featureless fluctuations with no periodic waveforms. The PSD_T plotted in coordinates of log₁₀ power vs. log₁₀ frequency often conforms to a straight line with slope ranging from near or below -2 (“brown” noise, 1/f²) in waking rest to near or below -3 (“black” noise, near 1/f³ (Schroeder, 1991)) in deep slow wave sleep (Freeman et al., 2006). When subjects become active, and often well before they do, excess power emerges above the straight line particularly in the classic theta (3–7 Hz), alpha (8–12 Hz), beta (12–25 Hz) and gamma ranges (30–80 Hz) (Fig. 2). These upward deviations manifest the breaking of the symmetry of unstructured random activity in disorder by the emergence of order in the spectral domain, giving the indication that within a collection of “resting” and “occult cogitating” and/or “self-referential processing” states there can be defined a *ground* state by its lack of spectral peaks reflecting scale-free random noise, which appears to be the form taken by basal brain activity from which order emerges (Freeman, 2006; Freeman and Zhai, in press).

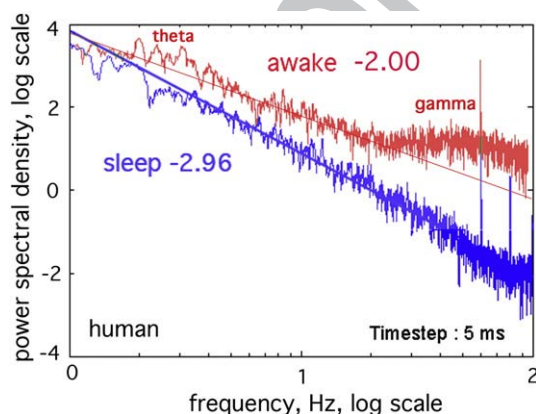


Fig. 2. The temporal power spectral density, PSD_T, in this human ECoG tends to a power-law distribution, 1/f^e, with exponent $e \sim 3 \pm .25$ in slow-wave sleep and $e \sim 2 \pm .25$ in the awake state (Freeman et al., 2006). Spectral peaks of excess power in the clinically significant bands (here gamma and low theta) during arousal and task performance. Adapted from (Freeman et al., 2006).

3.2. Deviations from the ground state to an active state by the emergence of order 459 460

This conclusion that the ECoG and EEG in the ground state conform to brown noise is consistent with the neural mechanism by which the background activity is maintained (reviewed in Freeman, 2008). The origin is in dense, distributed, mutual excitation among cortical excitatory neurons in positive feedback (Freeman, 1975, 2007b, 2008). Despite their sparseness, the interconnections are sufficiently dense that an action potential given by each neuron yields a prolonged barrage of action potentials from neighbors; that is, the anatomical connection density supports feedback gain that is potentially greater than unity. It is the refractory period of each neuron that prevents runaway excitation, so that large populations of cortical neurons self-stabilize homeostatically and sustain their activity in steady state at unity gain. This self-stabilized discharge is transmitted also to inhibitory interneurons. It provides the background excitation that inhibitory neurons require to exercise the mutual inhibition that supports spatial and temporal contrast enhancement by positive feedback to each other and the oscillations in the beta and gamma ranges by negative feedback to the excitatory neurons. Local feedback with short delays generates gamma rhythms that in gamma ECoG are synchronized over distances of 1 to 3 cm (Freeman, 2005a). Longer range feedback with greater delays typically gives rise to synchronized beta (Brovelli et al., 2004) and theta (Rizzuto et al., 2003) rhythms over larger distances (Freeman, 2005a,b). The inhibitory feedback does not stabilize cortex, nor do neural thresholds stabilize it; the factor that stabilizes the background fluctuations of EEG, MEG and ECoG is the refractory periods.

The level of power is not thereby constrained. Calculation of the probability of neural action potential formation conditional on the amplitude of the ECoG has shown that the background power is maintained in steady state at unity gain (Freeman, 2008) over a broad range of variation in level of arousal, which implicates the role of brain stem nuclei in neurohumoral control of the level of background activity. In the olfactory system the agent of increased background activity with arousal is histamine (Freeman, 2005a). Other systems appear to rely on other neuroamines. In any case the regulation of the ground state admits of two independent degrees of freedom relating to the level of arousal. One is the level of power that is assessed by the intercept of the line fitted to the PSD_T when it approaches the power-law form. The other is the robustness of the background activity, which is manifested as the slope of the PSD_T approaches -2 (Freeman and Zhai, in press).

There is no *a priori* reason to suppose that the power level of the ground state should be constant over time and spatially uniform throughout the brain at rest. To the contrary, the brain likely resembles the body, which has “catabolic” musculoskeletal systems that are quiescent during the actions of “anabolic” systems including the intestines, liver and kidneys. In turn the restorative organs shut down during intense muscular activity. Similarly there are likely to be brain regions and networks for which the main functions are anabolic in leisure or down time and others that support catabolic activities during intentional action. It is well known that blood flow is allocated between the two systems in the body largely according to strictly local demand. Similar local controls are known to exist in brains, conceivably giving the observed BOLD patterns (Raichle and Mintun, 2006). The mean level of power dissipation in brains is always high, owing to the necessity for maintaining a high-energy state near criticality (Freeman and Vitiello, 2006), so the question in any particular change of state is whether rate of dissipation necessarily increases with increased order in pattern formation. Indeed it may or may not. The separation between the two degrees of freedom is manifested in the independent variations of the slope and the intercept of the graph of log power versus log frequency (Freeman and Zhai, in press).

Therefore the $1/f$ criterion defines the “ground” state as requiring a state of “waking rest” with non-zero activity but without specifying its rate of energy expenditure. Certainly the “open loop” state that supervenes under deep anesthesia serves as a near-equilibrium “vacuum” state with zero background activity, from which the “ground” state emerges with recovery, and then on to the $1/f$ “waking rest” state as prelude to the “active” state with emergence of spectral structure (Skarda and Freeman, 1987). The “waking rest” state defined behaviorally may include some areas at the “ground” state defined spectrally and other areas in “active” states defined spectrally, so that departures from “waking rest” might incur increases and decreases from prevailing mean levels of activity (Raichle et al., 2001). A search for EEG and MEG peaks in the temporal PSD_T and spatial PSD_X “resting” state may yield clues to occult neural activity supporting mental activity that is undetected by observers or unreported by subjects because it is not conscious. The pass bands (widths and center frequencies) of the deviations from randomness ($1/f$ irrespective of slope) can give clues to start modeling the activities.

4. Search for spatial structures in EEG and MEG to combine with those in fMRI

Most non-invasive brain imaging studies of field potentials have been devoted to spatial localization of brain activity, including the use of PET/fMRI to guide MEG/EEG source imaging for improved spatiotemporal localization (Heinze et al., 1994; Menon et al., 1997; Liu et al., 1998; Ahlfors et al., 1999). Here we propose an alternative way to use the data from the three non-invasive brain imaging methods, namely the detection of spatial patterns of amplitude

modulation (AM) and phase modulation (PM) of *non-local*, transiently phase-locked oscillations in human brains.

4.1. Detecting spatial patterns of oscillatory activity in ECoG

The aim of brain imaging is to relate brain state to behavioral state through measurement by which the infinite state spaces is projected into a finite measurement spaces. The high-resolution measurements of the ECoG from arrays of electrodes fixed on the pial surface of cortex serve to sample infinite brain state in a series of spatial patterns of amplitude modulation (AM) and phase modulation (PM) of phase-locked oscillations in the beta and gamma ranges. The behavioral measurements project the infinite behavioral state space into discrete classes of CS and CR. The AM patterns are correlated with CS to which the subjects have been trained to give CR. Multivariate clustering and classification of AM patterns demonstrate the correlations between brain state and behavior state by projection into 2-space, i.e., a graphic display of clusters. Operationally, the amplitude of the signal from each of n spatial points in an array of n electrodes is calculated over a time segment. An n -dimensional feature vector is constructed from the n amplitudes that specify for each AM pattern a point in n -space. Similar AM patterns from repeated trials with the same CS form clusters of points. Differing AM patterns from trials with different CS form separate and partially overlapping clusters (Viana Di Prisco and Freeman, 1985; Ohl et al., 2001; Freeman and Burke, 2003; Freeman, 2005b). The trajectories between clusters describe the transitions between states.

The classificatory information in the ECoG is homogeneously distributed over the sensory cortex; no electrode gives a signal that is

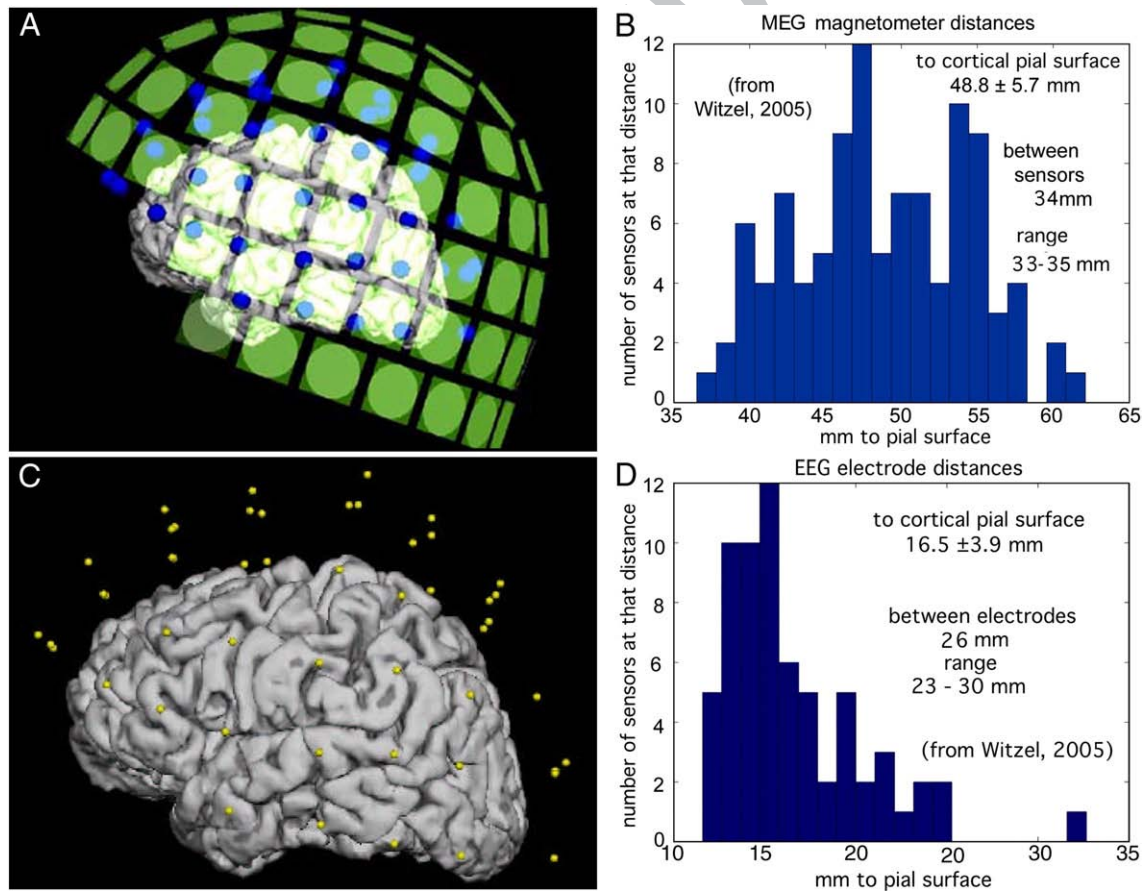


Fig. 3. A. Left lateral view of the locations of the MEG sensors (green squares) in relation to the pial surface of the cerebral cortex. The representation for the cortex was reconstructed from MR images. B. Histogram of MEG sensor distances to the nearest point on the pial surface. C. Left lateral view of the locations of EEG electrodes (yellow dots) relative to the cortex. D. Histogram of EEG electrode distances to the pial surface. (For interpretation of the references to colour in this figure legend, the reader is referred to the web version of this article.)

any more or less effective than any other (Barrie et al., 1996; Ohl et al., 2001), showing that the location of the electrodes is not critical, provided that the electrodes are all fixed within the area of spatial coherence of the carrier wave. Both low and high amplitudes of signals have equal value in classification, showing inclusiveness with respect to excitation, disexcitation, inhibition, and disinhibition in activation and de-activation. This generality reflects the distributed nature of the contents of holographic types of memory storage (Pribram, 1975). Each AM pattern is accompanied by a PM pattern, which is imposed by intracortical axonal conduction delays in the formation of each AM pattern. The phase dispersion at the peak frequency is within $\pm 45^\circ$; it shows that synchronization is widespread but not strictly at zero lag.

4.2. Extrapolation to search for spatiotemporal patterns in scalp EEG

The demonstration of the equal classificatory value of each channel in ECoG is extremely important for image analysis. The geometry of ECoG recording is comparatively simple; that for the EEG and MEG is not. The amplitude of the signal from each scalp sensor depends in part on the intrinsic intensities of the dendritic sources of the local current densities and also on the distances from those sources (Fig. 3), the orientations of the palisade of pyramidal cells as determined by the geometry of the gyri and sulci, and the conductances of the intervening skull and soft tissues. However, after the sensor array has been fixed to the head, the signal from each channel can be normalized to equal variance across the array for the data set that includes all behavioral conditions over which AM patterns are to be compared and classified. Then these several factors can be treated as invariant.

The AM patterns seen in the ECoG are stationary only for time segments lasting on the order of a tenth of a second. Each has an abrupt onset that is manifested in a temporal discontinuity of the analytic phase. When a jump in phase occurs at any one site, it tends to occur at all sites in the array, constituting what we call *coordinated analytic phase differences* (CAPD) that mark the onset of an AM pattern. These CAPD are also found in the EEG from 1-D arrays extending for distances up to 19 cm across the scalp (Freeman et al., 2003a). They suggest that comparable AM pattern formation by areas of cortex might simultaneously be manifested in electric, magnetic, and

hemodynamic images from extended cortical areas comprising gyri and sulci (Fig. 4). The important lesson here is that time averages must be taken across EEG and MEG data to combine with fMRI data, but not as is commonly done by averaging the time-dependent oscillations, because the variations in frequency and phase degrade the sums. Instead, the requirement is for temporal coarse-graining by identifying the AM patterns at whatever carrier frequencies and phase gradients they might have and saving only the feature vectors as points in n -space within the designated time frame.

4.3. Extrapolation to search for spatiotemporal patterns in MEG

Since the electric and magnetic fields of the MEG, EEG and ECoG share the same source in the dendritic currents of cortical pyramidal cells, we expected to find CAPD in the MEG as well. That we did not find them (Fig. 5) is quite instructive. In conformance with the law of charge conservation, dendritic currents flow in closed loops that cross the neural membranes twice. The ionic “battery” at the synapses has a high internal resistance that is matched by the high resistance at trigger zones. Most of the dendritic power is dissipated at these membrane crossings as heat, in proportion to the difference between the intracellular potential measured in millivolts compared with the extracellular potential measured in microvolts, a thousand-fold difference. The internal current is compressed into high density along the dendritic shafts in 1-D. The external current spreads widely in 3-D. A common misconception is that the extracellular current determines the EEG, while the intradendritic current determines the MEG. Actually both parts of the loop current determine the fields of both EEG and MEG, so that variations in extracellular resistance in opposite directions can reduce observed fields of potential by cancellation. Fortunately, although these complex details are critical for researchers who want to localize current sources, they are not needed for multivariate classification of AM patterns of EEG and MEG.

What is relevant to the missing CAPD is gyrification. The palisades of pyramidal cells are oriented perpendicular to the pial surface in both gyri and sulci. Sources of all orientations contribute to the EEG; however, the strongest contribution comes from the cortex in the

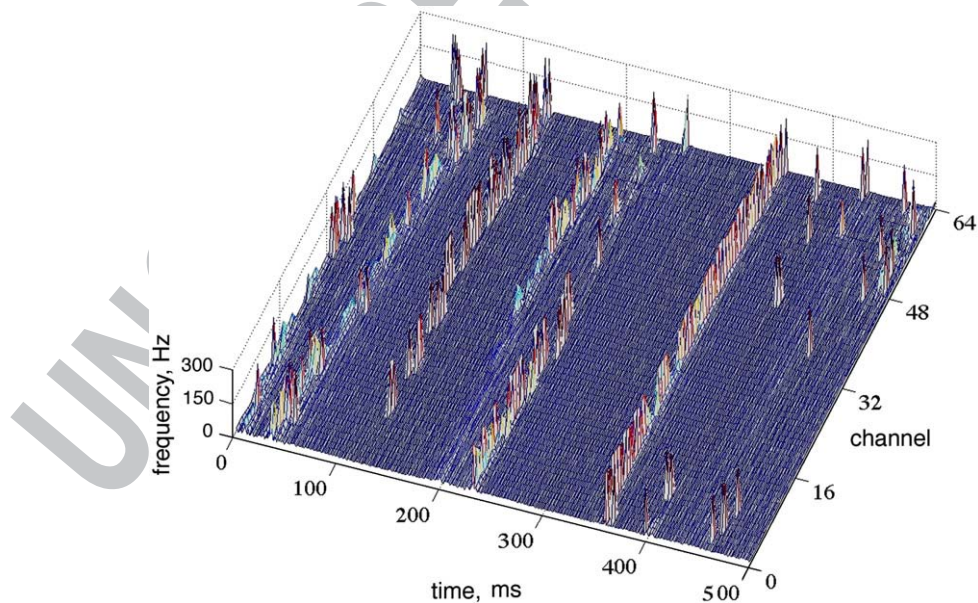


Fig. 4. The raster plot shows the CAPD from the scalp EEG of a human volunteer at rest with eyes closed. The array was 1-D across the occipital lobe from right to left in steps of 3 mm (total length: 189 mm). Pass band = 12–30 Hz; spacing = 3 mm. CAPD were calculated at the digitizing step $\Delta t = 5$ ms and aligned in rows parallel to the left abscissa. The flat areas show the stationarity of the phase within frames. The spikes aligned in rows parallel to the right abscissa show the spatial coordination of the phase discontinuities, often across both hemispheres (Freeman, 2004a).

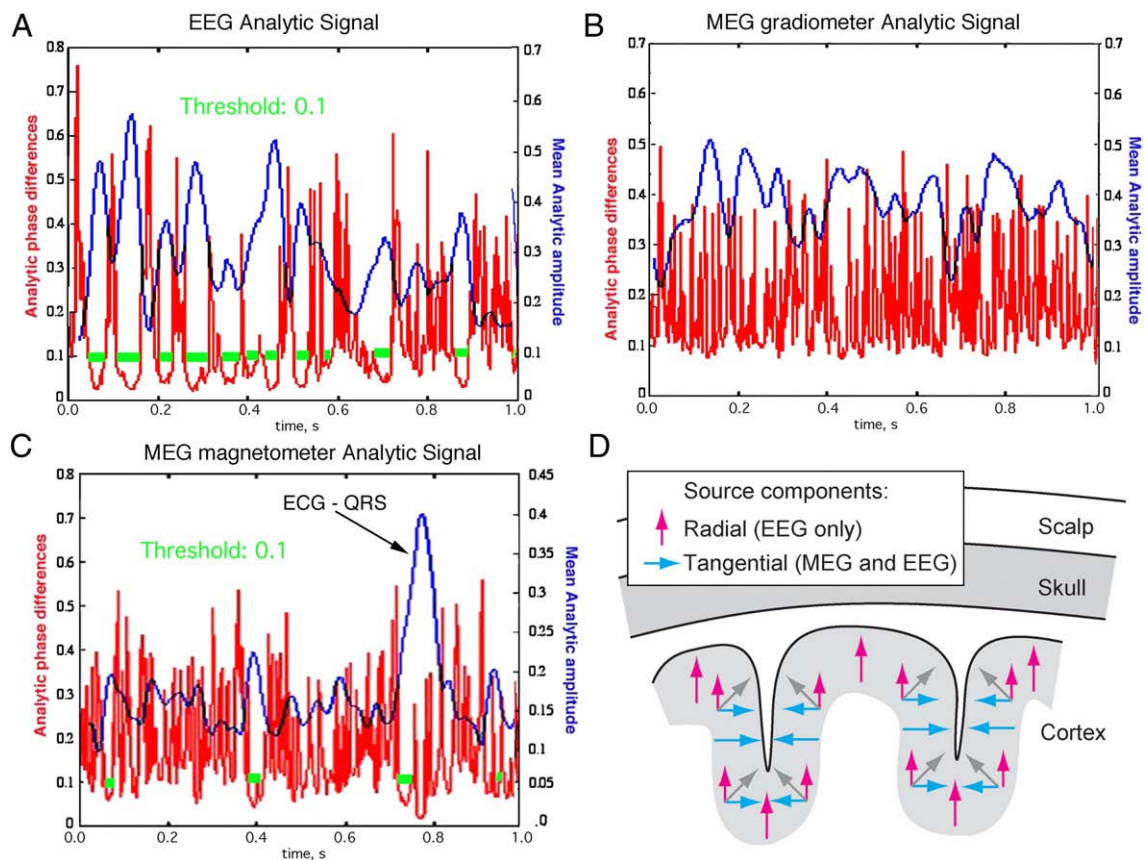


Fig. 5. The relationships are shown between analytic amplitude (smooth curves) and phase differences (spikes) in the beta range in non-invasive EEG (A), MEG gradiometers (B) and MEG magnetometers (C). The horizontal bars indicate the segments when the analytic phase difference was below 0.1 for at least 10 ms, suggesting the presence of CAPD. The large amplitude peak in MEG magnetometer data is an artifact due to cardiac magnetic field. D. The orientations of dipoles are schematized with respect to gyri and sulci in widely synchronized oscillatory potentials in the beta and gamma ranges for EEG (vertical arrows) and MEG (horizontal arrows). The signals from tangential source components (blue or black arrows) on opposite walls of sulci tend to cancel; this could explain why CAPD were not observed in the MEG recording.

crowns of gyri due to their closest distances to the scalp (Fig. 3) as well as the preferred orientation of the source currents. Conversely MEG is insensitive to source currents that are oriented perpendicular to the surface of the skull (*radial* sources, for example along the crests of the gyri). Therefore the strongest contribution to MEG signals typically originates from the tangentially oriented sources in sulci (Hillebrand and Barnes, 2002; Goldenholz et al., 2008), provided that the pyramidal cells in the opposing walls are synchronized, for in the synchronized case the opposing vectors tend to cancel. This may explain the finding that the CAPD do not appear in averaged signals derived from the MEG despite their appearance in averaged signals derived from the simultaneously recorded EEG (Fig. 5). The appearance of CAPD in EEG averages but not in MEG averages means that EEG will be especially important in providing markers for state transitions and frames in the search for AM patterns of analytic power (the maxima in the blue curves in Fig. 5A) to combine EEG and MEG for inclusion in the construction of global state variables. Power dissipation should be combined over the full spectral range in the steps required for application of the Hilbert transform to compute the analytic power in each frequency band.

5. Conclusion

To reiterate, in the detection and description of mesoscopic AM patterns, the spatial locations on the cortical surface of the peaks and troughs of analytic amplitude and their spatial boundaries are secondary. The identification is made by the locations in n -space of the AM patterns being classified by their Euclidean distances from the centers of gravity of clusters representing the classes. Only after an AM

pattern has been correlated with an aspect of cognitive behavior might it then be repeatedly induced and observed. The cortical domain within which it most probably originates can be mapped using a two-dimensional array of local electric and magnetic dipoles at the grain of the arrays, using the gyri and sulci revealed in structural MRI, so that the distributed sources contributing to an AM pattern of analytic power dissipation can be computed for each frequency range. The sum of power over the full frequency range and the time interval needed for reliable fMRI can be compared and coordinated with an fMRI map of power that has been computed with local averages corresponding to the sensor arrays.

The implication is that the brain state in any given time segment has the form of a spatial pattern of the rate of energy dissipation that is manifested in the three forms of imaging. Each state can be expressed in an AM pattern, in which every value, whether high or low, negative or positive, has equal value for purposes of description and classification. The nature of the state variables, whether electric, magnetic, or metabolic, may differ, but the value is independent of the source. The fMRI pattern in each macroscopic time interval at its time resolution provides an arena for analysis. The voxels can be selected to correspond to the neocortex and locally averaged spatially to coarse-grain the data in correspondence to the spatial resolution of the EEG and MEG data, which is determined by the sensor arrays. The high temporal resolution of the EEG and MEG gives repeated samples that cannot be summed as raw oscillations, but the clusters of points of their respective AM patterns can be accumulated over the time intervals dictated by the fMRI, so the basis for combining them is inherent in the spatial layout of the neocortex spread under the scalp and skull. The end result is the reduction of infinite brain state space to

a finite measurement space that is determined by the spatial sampling imposed on the EEG and MEG data and the temporal sampling that is imposed on the fMRI data. Multivariate statistics then supports projection of the finite state space into 2-space, a graph, in which each state may appear as a point, similar states as clusters, and state transitions as trajectories between clusters. Such macroscopic patterns are described as *metastability* (Kelso, 1995; Bressler and Kelso, 2001), itinerant trajectories (Tsuda, 2001), and cinematographic cortical dynamics (Freeman, 2007b).

Q5717 6. Uncited references

718 Bassett et al., 2006
 719 Buzsaki, 2006
 720 Emery and Freeman, 1969
 721 Fox et al., 2005
 722 Freeman, 2007a
 723 Freeman, 2007c
 724 Freeman and Rogers, 2003
 725 Freeman et al., 2008
 726 Freeman et al., in press
 727 Greicius and Menon, 2004
 728 Kozma and Freeman, 2001
 729 Pribram, 1971
 730 Rice, 1950
 731 Sacks, 2004

732 Acknowledgements

733 This study was supported by grant MH 06686 from the National
 734 Institute of Mental Health to WJF, grant NCC 2-1244 from the National
 735 Aeronautics and Space Administration, grant EIA-0130352 from the
 736 National Science Foundation to Robert Kozma, NIH grant NINDS-
 737 NS058899 to VM, and NIH grant NS057500 to SA. Programming was
 738 by Brian C. Burke. The MRI of the human subject was provided by Jeff
 739 H. Duyn and Tom Holroyd at the National Institute of Mental Health.
 740 We thank Sylvia Tomiyama for assistance with Fig. 1, Thomas Witzel
 741 for assistance with Fig. 3, and Maria Barth for assistance with the
 742 bibliography.

743 References

744 Ahlfors, S., Simpson, G., Dale, A., Belliveau, J., Liu, A., Korvenoja, A., et al., 1999.
 745 Spatiotemporal activity of a cortical network for processing visual motion revealed
 746 by MEG and fMRI. *J. Neurophysiol.* 82 (5), 2545–2555.
 747 Arieli, A., Grinvald, A., 2002. Optical imaging combined with targeted electrical recordings,
 748 microstimulation, or tracer injections. *J. Neurosci. Methods* 116 (1), 15–28.
 749 Baars, B.J., 1997. *In the Theater of Consciousness: The Workspace of the Mind*. Oxford U.P.,
 750 New York.
 751 Barrie, J., Freeman, W., Lenhart, M., 1996. Spatiotemporal analysis of prepyriform, visual,
 752 auditory, and somesthetic surface EEGs in trained rabbits. *J. Neurophysiol.* 76 (1),
 753 520–539.
 754 Bassett, D., Meyer-Lindenberg, A., Achard, S., Duke, T., Bullmore, E., 2006. Adaptive
 755 reconfiguration of fractal small-world human brain functional networks. *Proc. Natl.*
 756 *Acad. Sci. U.S.A.* 103 (51), 19518–19523.
 757 Bressler, S.L., Kelso, J.A.S., 2001. Cortical coordination dynamics and cognition. *Trends*
 758 *Cogn. Sci.* 5, 26–36.
 759 Bressler, S., Richter, C., Chen, Y., Ding, M., 2007. Cortical functional network organization
 760 from autoregressive modeling of local field potential oscillations. *Stat. Med.* 26 (21),
 761 3875–3885.
 762 Brovelli, A., Ding, M., Ledberg, A., Chen, Y., Nakamura, R., Bressler, S., 2004. Beta
 763 oscillations in a large-scale sensorimotor cortical network: directional influences
 764 revealed by Granger causality. *Proc. Natl. Acad. Sci. U.S.A.* 101 (26), 9849–9854.
 765 Buckner, R., Andrews-Hanna, J., Schacter, D., 2008. The brain's default network:
 766 anatomy, function, and relevance to disease. *Ann. N.Y. Acad. Sci.* 1124, 1–38.
 767 Buzsaki, G., 2006. *Rhythms of the Brain*. Oxford UP, New York.
 768 Buzsáki, G., Kaila, K., Raichle, M., 2007. Inhibition and brain work. *Neuron* 56 (5), 771–783.
 769 Emery, J., Freeman, W., 1969. Pattern analysis of cortical evoked potential parameters
 770 during attention changes. *Phys. Behav.* 4, 67–77.
 771 Fox, P., Raichle, M., Mintun, M., Dence, C., 1988. Nonoxidative glucose consumption
 772 during focal physiologic neural activity. *Science* 241 (4864), 462–464.

Fox, M.D., Snyder, A.Z., Vincent, J.L., Corbetta, M., Van Essen, D.C., Raichle, M.E., 2005. 773
 The human brain is intrinsically organized into dynamic, anticorrelated functional 774
 networks. *Proc. Natl. Acad. Sci. U.S.A.* 102 (27), 9673–9678. 775
 Franssen, P., 2006. How default is the default mode of brain function? Further evidence 776
 from intrinsic BOLD fluctuations, vol. 44, pp. 2836–2845. 777
 Freeman, W., 1975. *Mass Action in the Nervous System*. Academic Press, New York. 778
 Freeman, W., 2004a. Origin, structure, and role of background EEG activity. Part 1. 779
 Analytic amplitude. *Clin. Neurophysiol.* 115 (9), 2077–2088. 780
 Freeman, W., 2004b. Origin, structure, and role of background EEG activity. Part 2. 781
 Analytic phase. *Clin. Neurophysiol.* 115 (9), 2089–2107. 782
 Freeman, W., 2005a. NdN, volume transmission, and self-organization in brain dynamics. 783
J. Integr. Neurosci. 4 (4), 407–421. 784
 Freeman, W., 2005b. Origin, structure, and role of background EEG activity. Part 3. 785
 Neural frame classification. *Clin. Neurophysiol.* 116 (5), 1118–1129. 786
 Freeman, W., 2006. Origin, structure, and role of background EEG activity. Part 4: Neural 787
 frame simulation. *Clin. Neurophysiol.* 117 (3), 572–589. 788
 Freeman, W., 2007a. Indirect biological measures of consciousness from field studies of 789
 brains as dynamical systems. *Neural Netw.* 20 (9), 1021–1031. 790
 Freeman, W., 2007b. Proposed cortical “shutter” mechanism in cinematographic perception. 791
 In: Perlovsky, L., Kozma, R. (Eds.), *Neurodynamics of Cognition and Consciousness*. 792
 Springer Verlag, Heidelberg, pp. 11–38. 793
 Freeman, W., 2007c. *Encyclopedia for Computational Neuroscience*. http://www.scholarpedia.org/article/Hilbert_transform_for_brain_waves. 794
 Freeman, W., 2008. A pseudo-equilibrium thermodynamic model of information 795
 processing in nonlinear brain dynamics. *Neural Netw.* 21 (2–3), 257–265. 797
 Freeman, W., Burke, B., 2003. A neurobiological theory of meaning in perception. Part 798
 4. Multicortical patterns of amplitude modulation in gamma EEG. *Int. J. Bifurc.* 799
Chaos 13, 2857–2866. 800
 Freeman, W., Rogers, L., 2003. A neurobiological theory of meaning in perception. Part 5. 801
 Multicortical patterns of phase modulation in gamma EEG. *Int. J. Bifurc. Chaos* 13, 802
 2867–2887. 803
 Freeman, W., Vitiello, G., 2006. Nonlinear brain dynamics as macroscopic manifesta- 804
 tion of underlying many-body field dynamics. *Phys. Life Rev.* 3, 93–118. 805
 Freeman, W., & Zhai, J., in press. Simulated power spectral density (PSD) of background 806
 electrocorticogram (ECoG). *Cogn. Neurodynamics*. 807
 Freeman, W., Rogers, L., Holmes, M., Silbergeld, D., 2000. Spatial spectral analysis of 808
 human electrocorticograms including the alpha and gamma bands. *J. Neurosci.* 809
Methods 95 (2), 111–121. 810
 Freeman, W., Burke, B., Holmes, M., 2003a. Aperiodic phase re-setting in scalp EEG of 811
 beta-gamma oscillations by state transitions at alpha-theta rates. *Hum. Brain Mapp.* 812
19 (4), 248–272. 813
 Freeman, W., Holmes, M., Burke, B., Vanhatalo, S., 2003b. Spatial spectra of scalp EEG 814
 and EMG from awake humans. *Clin. Neurophysiol.* 114 (6), 1053–1068. 815
 Freeman, W., Holmes, M., West, G., Vanhatalo, S., 2006. Fine spatiotemporal structure of 816
 phase in human intracranial EEG. *Clin. Neurophysiol.* 117 (6), 1228–1243. 817
 Freeman, W.J., Bollobás, B., Kozma, R., 2008. Scale-free cortical planar networks. 818
Handbook of Large-scale Random Networks. Bolyai Mathematical Soci. Springer, 819
 Budapest. <http://www.springer.com/math/numbers/book/978-3-540-69394-9>. 820
 Freeman, W., O’Nuallain, S., Rodriguez, J., in press. Simulating resting cortical 821
 background activity with filtered noise. *J. Integr. Neurosci.* 822
 Goense, J., Logothetis, N., 2008. Neurophysiology of the BOLD fMRI signal in awake monkeys. 823
Curr. Biol. 18 (9), 631–640. 824
 Goldenholz, D., Ahlfors, S., Hämäläinen, M., Sharon, D., Ishitobi, M., Vaina, L., et al., 2008. 825
 Mapping the signal-to-noise-ratios of cortical sources in magnetoencephalography 826
 and electroencephalography. *Hum. Brain Mapp.* 827
 Greicius, M.D., Menon, V., 2004. Default-mode activity during a passive sensory task: 828
 uncoupled from deactivation but impacting activation. *J. Cogn. Neurosci.* 16 (9), 829
 1484–1492. 830
 Greicius, M.D., Krasnow, B., Reiss, A.L., Menon, V., 2003. Functional connectivity in the 831
 resting brain: a network analysis of the default mode hypothesis. *Proc. Natl. Acad.* 832
Sci. U.S.A. 100 (1), 253–258. 833
 Haynes, J., Rees, G., 2006. Decoding mental states from brain activity in humans. *Nat.* 834
Rev. Neurosci. 7 (7), 523–534. 835
 Heinze, H., Mangun, G., Burchert, W., Hinrichs, H., Scholz, M., Münte, T., et al., 1994. 836
 Combined spatial and temporal imaging of brain activity during visual selective 837
 attention in humans. *Nature* 372 (6506), 543–546. 838
 Herrmann, C., Debener, S., 2008. Simultaneous recording of EEG and BOLD responses: a 839
 historical perspective. *Int. J. Psychophysiol.* 67 (3), 161–168. 840
 Hillebrand, A., Barnes, G., 2002. A quantitative assessment of the sensitivity of whole- 841
 head MEG to activity in the adult human cortex. *Neuroimage* 16 (3 Pt 1), 638–650. 842
 Kelso, J.A.S., 1995. *Dynamic Patterns: The Self Organization of Brain and Behavior*. MIT 843
 Press, Cambridge. 844
 Kozma, R., Freeman, W., 2001. Methods and applications for robust classification of 845
 noisy and variable patterns. *Int. J. Bifurc. Chaos* 10, 2307–2322. 846
 Liu, A., Belliveau, J., Dale, A., 1998. Spatiotemporal imaging of human brain activity 847
 using functional MRI constrained magnetoencephalography data: Monte Carlo 848
 simulations. *Proc. Natl. Acad. Sci. U.S.A.* 95 (15), 8945–8950. 849
 Logothetis, N., 2008. What we can do and what we cannot do with fMRI. *Nature* 453 850
 (7197), 869–878. 851
 Logothetis, N.K., Pfeuffer, J., 2004. On the nature of the BOLD fMRI contrast mechanism. 852
Magn. Reson. Imaging 22 (10), 1517–1531. 853
 Makeig, S., Westerfield, M., Jung, T.P., Enghoff, S., Townsend, J., Courchesne, E., 854
 Sejnowski, T.J., 2002. Dynamic brain sources of visual evoked responses. *Science* 855
 295, 690–694. 856
 Menon, V., Crottaz-Herbette, S., 2005. Combined EEG and fMRI studies of human 857
 brain function. *Int. Rev. Neurobiol.* 66, 291–321. 858

- 859 Morcom, A., Fletcher, P., 2007. Does the brain have a baseline? Why we should be
860 resisting a rest. *Neuroimage* 37 (4), 1073–1082.
- 861 Niedermeyer, E., Lopes da Silva, F.H., 2004. *Electroencephalography: Basic principles,*
862 *Clinical Applications, and Related Fields*, 5th ed. Lippincott Williams & Wilkins,
863 Philadelphia.
- 864 Northoff, G., Heinzel, A., De Greck, M., Bormpohl, F., Dobrowolny, H., Panksepp, J., 2006.
865 Self-referential processing in our brain—a meta-analysis of imaging studies of the
866 self. *Neuroimage* 31, 440–457.
- 867 Ohl, F.W., Scheich, H., Freeman, W.J., 2001. Change in pattern of ongoing cortical activity
868 with auditory category learning. *Nature* 412, 733–736.
- 869 Panagiotides, H., Freeman, W.J., Holmes, M.D., Pantazis, D., 2008. Behavioral states
870 exhibit distinct spatial EEG patterns. Abstract #1.051, 62nd Ann. Mtg., Amer.
871 Epilepsy Soc., Seattle WA.
- 872 Pfurtscheller, G., Cooper, R., 1975. Frequency dependence of the transmission of the EEG
873 from cortex to scalp. *Electroencephalogr. Clin. Neurophysiol.* 38 (1), 93–96.
- 874 Pribram, K.H., 1971. *Languages of the Brain: Experimental Paradoxes and Principles in*
875 *Neuropsychology*. Prentice-Hall, Englewood Cliffs, NJ. Monterey.
- 876 Pribram, K., 1975. The primate frontal cortex: progress report 1975. *Acta Neurobiol. Exp.*
877 35 (5–6), 609–625 (Wars).
- 878 Raichle, M., 2006. Neuroscience. The brain's dark energy. *Science* 314 (5803),
879 1249–1250.
- 880 Raichle, M., Mintun, M., 2006. Brain work and brain imaging. *Annu. Rev. Neurosci.* 29,
881 449–476.
- 882 Raichle, M., Snyder, A., 2007. A default mode of brain function: a brief history of an
883 evolving idea. *Neuroimage* 37 (4), 1083–1090 discussion 1097–1089.
- 884 Raichle, M.E., MacLeod, A.M., Snyder, A.Z., Powers, W.J., Gusnard, D.A., Shulman, G.L.,
885 2001. A default mode of brain function. *Proc. Natl. Acad. Sci. U. S. A.* vol. 98 (2),
886 676–682.
- 887 Ramon, C., Schimpf, P., Hauelsen, J., Holmes, M., Ishimaru, A., 2004. Role of soft bone, CSF
888 and gray matter in EEG simulations. *Brain Topogr.* 16 (4), 245–248.
- 889 Rice, S.O., 1950. *Mathematical Analysis of Random Noise—and Appendixes—Technical*
890 *Publications Monograph B-1589*. Bell Telephone Labs, New York.
- 891 Rizzuto, D., Madsen, J., Bromfield, E., Schulze-Bonhage, A., Seelig, D., Aschenbrenner-
892 Scheibe, R., et al., 2003. Reset of human neocortical oscillations during a working
893 memory task. *Proc. Natl. Acad. Sci. U. S. A.* 100 (13), 7931–7936.
- Sacks, O., 2004. *In the River of Consciousness*. Review, New York. 51(1). 894
- Schacter, D.L., Addis, D.R., 2007. The cognitive neuroscience of constructive memory:
895 remembering the past and imagining the future. *Phil. Trans. Roy. Soc. (B)* 362, 896
773–786. 897
- Schroeder, M., 1991. *Fractals, Chaos, Power Laws*. WH Freeman, San Francisco. 898
- Schummers, J., Yu, H., Sur, M., 2008. Tuned responses of astrocytes and their influence
899 on hemodynamic signals in the visual cortex. *Science* 320 (5883), 1638–1643. 900
- Shulman, G.L., Fiez, J.A., Corbetta, M., Buckner, R.L., Miezin, F.M., Raichle, M.E., et al.,
901 1997. Common blood flow changes across visual tasks: II. Decreases in cerebral
902 cortex. *J. Cogn. Neurosci.* 9, 648–663. 903
- Singer, W., 2001. Consciousness and the binding problem. *Ann. N.Y. Acad. Sci.* 929, 904
123–146. 905
- Skarda, C.A., Freeman, W.J., 1987. How brains make chaos in order to make sense of the
906 world. *Behav. Brain Sci.* 10 (2), 161–195. 907
- Soon, C., Brass, M., Heinze, H., Haynes, J., 2008. Unconscious determinants of free
908 decisions in the human brain. *Nat. Neurosci.* 11 (5), 543–545. 909
- Szpunar, K.K., Watson, J.M., McDermott, K.B., 2007. Neural substrates of envisioning the
910 future. *Proc. Natl. Acad. Sci.* 104, 642–647. 911
- Tsuda, I., 2001. Towards an interpretation of dynamic neural activity in terms of chaotic
912 dynamical systems. *Behav. Brain Sci.* 24, 793–810. 913
- Viana Di Prisco, G., Freeman, W.J., 1985. Odor-related bulbar EEG spatial pattern analysis
914 during appetitive conditioning in rabbits. *Behav. Neurosci.* 99, 962–978. 915
- Viswanathan, A., Freeman, R., 2007. Neurometabolic coupling in cerebral cortex reflects
916 synaptic more than spiking activity. *Nat. Neurosci.* 10 (10), 1308–1312. 917
- Wolf, F., Kirchhoff, F., 2008. Neuroscience. Imaging astrocyte activity. *Science* 320
918 (5883), 1597–1599. 919
- Worsely, K.J., 2005. Spatial smoothing of autocorrelations to control the degrees of
920 freedom in fMRI analysis. *Neuroimage* 26 (2), 635–642 PMID: 15907321 [PubMed—
921 indexed for MEDLINE]. 922
- Zhou, H., van Oosterom, A., 1992. Computation of the potential distribution in a four-
923 layer anisotropic concentric spherical volume conductor. *IEEE Trans. Biomed. Eng.*
924 39 (2), 154–158. 925